

**High-glucose toxicity is mediated by AICAR-transformylase/IMP cyclohydrolase and mitigated by AMP-activated protein kinase in *Caenorhabditis elegans***

Christin Riedinger<sup>1\*</sup>, Michael Mendler<sup>1\*</sup>, Andrea Schlotterer<sup>1</sup>, Thomas Fleming<sup>1</sup>, Jürgen Okun<sup>2</sup>, Hans-Peter Hammes<sup>3</sup>, Stephan Herzig<sup>4/5/6</sup> and Peter P. Nawroth<sup>1/5/6</sup>

<sup>1</sup>Department of Medicine I and Clinical Chemistry, University of Heidelberg, Im Neuenheimer Feld 410, 69120 Heidelberg, Germany

<sup>2</sup>Department of Pediatric, Dietmar-Hopp-Metabolism Centre, Heidelberg, Germany

<sup>3</sup>V. Medical Hospital, University Hospital Mannheim, Theodor-Kutzer-Ufer 1-3, 68167 Mannheim, Germany

<sup>4</sup>Institute for Diabetes and Cancer IDC, Helmholtz Center Munich, Ingolstädter Landstraße 1, 85764 Neuherberg, Germany

<sup>5</sup>Joint Heidelberg IDC Translational Diabetes Program, Heidelberg University Hospital, Im Neuenheimer Feld 410, 69120 Heidelberg, Germany

<sup>6</sup>German Center for Diabetes Research (DZD), Ingolstädter Landstraße 1, 85764 Neuherberg, Germany

\* C. Riedinger and M. Mendler contributed equally to the manuscript

Running title: Protective Effect of AICAR under High Glucose

Corresponding author: Prof. Dr. med. Dr. h.c. Peter Paul Nawroth, Department of Medicine I and Clinical Chemistry, University of Heidelberg, Im Neuenheimer Feld 410, 69120 Heidelberg, Phone: +49 6221 56-8601, Fax: +49 6221 56-5587, E-Mail: [peter.nawroth@med.uni-heidelberg.de](mailto:peter.nawroth@med.uni-heidelberg.de)

Keywords: AICAR, AMP-activated kinase (AMPK), ATIC, *Caenorhabditis elegans* (*C. elegans*), diabetes, DNA damage; reactive oxygen species (ROS)

---

**ABSTRACT**

The enzyme AICAR-transformylase/IMP cyclohydrolase (ATIC) catalyzes the last two steps of purine de-novo synthesis. It metabolizes AICAR, which is an AMP analogue, leading to activation of AMPK. It was investigated whether the AICAR-ATIC pathway plays a role in the high glucose (HG) mediated DNA damage response and AICAR mediated AMPK activation, explaining the detrimental effects of glucose on neuronal damages and shortening of lifespan. HG up-regulated the expression and activity of *Caenorhabditis elegans* homologue of ATIC, C55F2.1 (*atic-1*), as well as increased the levels of reactive oxygen species (ROS) and methylglyoxal-

derived advanced glycation endproducts (MG-AGEs). Overexpression of *atic-1* decreased lifespan and head motility and increased neuronal damage under both standard (S) and high glucose (HG) conditions.

Inhibition of *atic-1* expression, by RNAi, under HG was associated with increased lifespan and head motility and reduced neuronal damage, ROS and MG-AGE accumulation. This effect was independent of an effect on DNA damage or antioxidant defense pathways, such as superoxide dismutase (*sod-3*) or glyoxalase-1 (*glod-4*), but was dependent upon AMPK and an accumulation of AICAR. Through AMPK, AICAR treatment also reduced the negative effects of HG. The

mitochondrial inhibitor rotenone abolished the AICAR/AMPK-induced amelioration of HG effects, pointing to mitochondria as a prime target of the glucotoxic effects in *C. elegans*. We conclude that *atic-1* is involved in glucotoxic effects under HG conditions, either by blocked *atic-1* expression or via AICAR and AMPK induction.

---

The enzyme AICAR-transformylase/IMP cyclohydrolase (ATIC) catalyzes the last two steps of purine de-novo synthesis. ATIC metabolites 5-Aminoimidazole-4-carboxamide-riboside (AICAR) to N-formyl-5-aminoimidazol-4-carboxamide-ribonucleotide (FAICAR) and then to inosine monophosphate (IMP), analog of adenosine monophosphate (AMP). IMP can then be phosphorylated by adenosine kinase to become ZMP, which can bind to the cystathionine-beta-synthase (CBS) domains of the  $\gamma$ -subunit of AMP-activated protein kinase (AMPK), leading to an allosteric change [(1)]. This change makes AMPK a better substrate for its upstream kinases to phosphorylate it at Thr172 and inhibits dephosphorylation at this site by the protein phosphatases, PP2A and PP2C [(2); (3)]. This combined effect significantly increases the activity of AMPK *ex vivo* [(4)].

Treatment with AICAR has been shown to prevent and/or reverse metabolic syndrome in animal models. In ob/ob mice, fa/fa rats, as well as rats fed on a high-fat diet, AICAR treatment has been shown to improve glucose tolerance, whole-body glucose disposal, as well as reduce hepatic glucose output and plasma triglycerides and free fatty acids levels [(5); (6); (7); (8)]. In streptozotocin (STZ)-induced diabetic mice, treatment with AICAR increased AMPK activity within the kidney and was linked with reduction in glomerular matrix and albuminuria [(9)]. Exogenous AICAR can therefore be considered to be an activator of AMPK *in vitro*. However, the regulation of ATIC by endogenous AICAR and its relationship to the activation of AMPK remains unknown, particularly within the context of the hyperglycemia and diabetes.

The regulation of AMPK is of great interest in the study of diabetes and metabolic syndrome as

evidence would suggest that loss and/or reduction of AMPK signaling plays an important role in the development of insulin resistance. Upon activation, AMPK signals through its downstream substrates to restore normal energy levels by stimulating metabolic processes that generate ATP, such as fatty acid oxidation, or by inhibiting those that use ATP, such as triglyceride and protein synthesis [(10)]. The formation of reactive metabolites such as reactive oxygen species (ROS) and methylglyoxal (MG) are closely linked to energy homeostasis. The normalization of the energy levels, induced by AMPK activation, would therefore provide an indirect means of defense against reactive metabolites. Indeed, it has been shown that activation of AMPK can decrease the production of ROS, by improving mitochondrial dysfunction *in vitro* and *in vivo*, as well in patients with diabetes [(11); (12); (13); (14); (15); (16)]. The treatment with AICAR was shown to rescue mitochondrial biogenesis, pyruvate dehydrogenase activity and mitochondrial complex activity in diabetic kidney [(9)]. Interestingly, the treatment of AICAR also normalized the production of superoxide, which was found to be reduced in the diabetic kidney. This would be consistent with the concept of mitochondrial hormesis or *mitohormesis*, in which a degree of ROS production is required within a given biological system to improve systemic defenses against such cellular stressors, by inducing an adaptive response [(11)].

Several studies have shown that DNA damage, from reactive metabolites [(17); (18); (19); (20)], play an important role in the development of late diabetic complications [(21); (22); (17); (18); (23); (24)]. Increased damage to the DNA would result in an increased demand on repair processes, in particularly the purine building blocks required for the DNA structure. Within the context of diabetes this is particularly relevant as there is evidence to suggest that diabetic patients have inefficient DNA repair [(25); (26)]. Within the context of the ATIC-AICAR pathway, it is conceivable that the activation of ATIC would be protective as it would provide the necessary pool of purines required for DNA repair. However, in doing so, the endogenous AICAR would be depleted leading to the loss of AMPK activation and the subsequent beneficial effects in reducing the production and/or consequences of reactive metabolites. The imbalance between the two functions of the ATIC-

AICAR pathway may therefore represent an important mechanism for the development the cellular dysfunction observed under hyperglycemic conditions.

In this study the effect of high glucose on ATIC, as well as the effect of AICAR on the activation of AMPK and the production of reactive metabolites and DNA damage was studied. As both AMPK and ATIC are conserved throughout evolution, *C. elegans* were used an easily accessible model system.

## RESULTS

The *C. elegans* homolog of *atic-1*, C55F2.1, was identified by *in silico* analysis. To verify its enzymatic function, a transgenic nematode (tgC55F2.1b) was created, and the activity of AICAR formyltransferase (AICARFT) was determined. This activity was increased in tgC55F2.1b from  $17.2 \pm 2.9$   $\mu\text{mol}/\text{min}$  to  $34.2 \pm 2.1$   $\mu\text{mol}/\text{min}$  ( $p=0.003$ ) when compared to WT, which corresponds well to the activity of the recombinant human protein (to  $43.5 \pm 1.8$   $\mu\text{mol}/\text{min}$ ;  $p=0.010$ ) (Fig.1A). A putative methylglyoxal-synthase domain was identified within C55F2.1, however, never the neither the protein extracts of the tg-nematodes, nor a commercially available purified enzyme of the human homologue, enhanced methylglyoxal (MG) production (Fig.1B).

Stimulation of WT nematodes with high glucose (HG), for five days, lead to an increase in the expression of *atic-1* of 2.4-fold, as compared to standard (S) conditions ( $p<0.049$ ) (Fig.1C). This increase in expression was found to persist up to 12 days under HG conditions; however, the effect was not dose-dependent with respect to glucose and not as consequence of osmotic effects (Supplementary Figure 1). The increased expression observed at five days of HG was reflected by an increase in AICARFT activity of ca. 2.7-fold as compared to S conditions (Fig.1D).

### Effect of *atic-1* over-expression

The effect of *atic-1* (C55F2.1b) overexpression on lifespan and neuronal damage was determined under standard (S) and high glucose (HG) conditions. Overexpression of *atic-1* decreased

median lifespan from  $23.6 \pm 0.9$  days to  $20.6 \pm 0.6$  days ( $p=0.004$ ), as compared to control nematodes under S conditions (Fig.2A). Under HG, the head motility of the WT nematodes was decreased by  $0.03 \pm 0.01$  mm/s ( $p=0.006$ ) as compared to S conditions ( $0.016 \pm 0.02$  m/s). Overexpression of *atic-1* decreased head mobility, non-significantly, under the S condition by  $0.03 \pm 0.02$  mm/s as compared to the WT nematodes under S conditions. HG treatment of the transgenic nematodes further reduced head motility by  $0.08 \pm 0.01$  mm/s ( $p=0.012$ ) as compared to WT nematodes under HG conditions (Fig.2B). Thus, the effect of HG on head motility was exaggerated in *atic-1* overexpressing *C. elegans*.

With respect to neuronal damage, HG increased the neuronal damage score from  $0.5 \pm 0.13$  to  $1.3 \pm 0.23$  ( $p=0.010$ ) in WT nematodes. Overexpression of *atic-1* increased the damage score to  $1.2 \pm 0.16$  ( $p=0.070$ ), as compared to the WT nematodes under S conditions. The damage score in *atic-1* transgenic nematodes was not enhanced by HG ( $p=0.761$ ) (Fig.2C+D). Thus, *atic-1* overexpression, under S conditions, was able to partially reduce lifespan, neuronal function and integrity and increased the C55F2.1b mRNA expression (Supplementary Figure 2).

### Protective effect of *atic-1* silencing

The up-regulation of *atic-1* in part mimicked the effects of HG. Therefore a protection from the effect of HG would be expected when the glucose-dependent induction of *atic-1* was inhibited. RNAi treatment of *atic-1* was verified by qPCR and decreased mRNA expression to  $24.9 \pm 11.3\%$  ( $p=0.003$ ) under S conditions and to  $35.6 \pm 14.3\%$  ( $p=0.011$ ) under HG conditions, as compared to WT nematodes (Supplementary Figure 3). The down-regulation of *atic-1* increased lifespan under HG conditions from  $11.0 \pm 0.5$  days to  $14.7 \pm 0.9$  days ( $p<0.0001$ ) (Fig.3A), while there was no effect under S conditions ( $p=0.427$ , data not shown). Head motility of control RNAi treated nematodes was decreased under HG conditions from  $0.15 \pm 0.01$  mm/s to  $0.10 \pm 0.01$  mm/s ( $p=0.019$ ). Under S conditions, the down-regulation of *atic-1* has no effect on head motility, as compared to the control RNAi treated nematodes. Under HG conditions, the down-regulation of *atic-1* prevented the decrease in head

motility observed in the control RNAi treated nematodes (Fig.3B). Consistent with the previous finding, HG increased the neuronal damage score from  $0.82\pm 0.07$  to  $1.42\pm 0.06$  ( $p=0.003$ ) in the control RNAi nematodes, which was prevented by the down-regulation of *atic-1* (Fig.3C).

With respect to the formation of ROS and dicarbonyls, HG increased ROS formation in the control RNAi nematodes from  $59\pm 13$  AU/pixel to  $222\pm 9$  AU/pixel ( $p=0.0001$ ), which was prevented by the down-regulation of *atic-1* (Fig.3D). Similar effects were also observed for the formation of MG-derived AGEs (Fig.3E).

As AICAR is the substrate of ATIC, it was hypothesized that the beneficial effect resulting from the down-regulation of *atic-1* was mediated by an accumulation of AICAR. There was no significant effect of HG on intracellular AICAR concentration ( $p=0.074$ ), however the amount of AICAR was close to the limit of detection. Interestingly, the down-regulation of *atic-1* increased intracellular AICAR by ca.8-fold under S conditions and ca.13.1-fold under HG conditions, as compared to the control nematodes. There was no significant difference in the intracellular AICAR concentration between the S and HG conditions in *atic-1* RNAi treated nematodes. This might indirectly reflect the basal turnover of AICAR by *atic-1*, suggesting that the baseline *atic-1* dependent AICAR turnover is saturated. This would be consistent with the findings observed with the overexpression of *atic-1*, which did not show any effect on the intracellular AICAR under S or HG conditions, as compared to the control nematodes (Fig.4A).

The lack of HG to reduce AICAR significantly is consistent with the failure of HG to induce DNA double strand breaks (ds-breaks), as measured by the comet assay. Using bleomycin treated WT nematodes as a positive control (Fig 4B), it was found that there was no significant difference in ds-break formation between S (Fig.4C) and HG (Fig.4D) conditions (Fig.4E, lane 3). Overexpression of *atic-1* did not reduce the formation of ds-breaks, as compared to control under S conditions ( $p>0.05$ ) (Fig.4E, lane 4), but did reduce ds-breaks under HG conditions to 5.6% ( $p=0.002$ ) (Fig.4E, lane 5). Under control RNAi conditions ds-breaks decreased under S conditions

(7.1%,  $p=0.003$ ) (Fig.4E, lane 6), while HG did not induce ds-breaks ( $p=0.600$ ) (Fig.4E, lane 7). The down-regulation of *atic-1* increased the formation of ds-breaks under S conditions by 21.9% ( $p=0.003$ ) (Fig.4E, lane 8), but for unknown reasons, glucose did not increase ds-breaks under HG conditions (14.7%,  $p>0.05$ ) (Fig.4E, lane 9). This was consistent with HG does not exert its toxic effect in nematodes via genomic DNA damage. Nevertheless, it can be concluded that, blocking *atic-1* expression enhanced DNA damage under S conditions, while overexpressing *atic-1* reduced DNA damage more under HG. However, as there were no significant differences between S and HG in WT nematodes, HG mediated *atic-1* induction and DNA damage does not seem to be an important pathway in explaining the *atic-1* induction related to the effects of HG.

#### *aak-2* dependent effect of *atic-1* silencing

To establish the potential mechanism for the effect of *atic-1*, the downstream signaling pathway was investigated using *aak-2* nematodes, a homolog of the catalytic subunit of AMPK. It was found that the effects resulting from the down-regulation of *atic-1* under HG conditions was dependent upon *aak-2* as there was no effect resulting from down-regulation of *atic-1* on lifespan in *aak-2* nematodes (Fig.5A). Furthermore, HG decreased head motility was not improved (Fig.5B). With respect to the formation of reactive metabolites, ROS formation was increased under HG condition from  $60\pm 10$  AU/pixel to  $221\pm 3$  AU/pixel ( $p<0.0001$ ) in the *aak-2* nematodes and was unaffected by down-regulation of *atic-1* (Fig.5C). Similar results were also found for MG-derived AGEs (Fig.5D). Thus, lack of AMPK abrogated the positive effects of *atic-1* suppression on lifespan, head motility and reactive metabolite accumulation.

#### Protective effect of AICAR

As the suppression of *atic-1* increased AICAR levels (Fig.4A and Supplementary Figure 4) a pharmacological approach was used to better understand the AICAR effect further. Stimulation of WT nematodes with high glucose (HG), for five days, led to a decrease in AMPK activity, an effect which was partially normalized by the exogenous addition of 1mM AICAR (Fig. 6A).

The HG mediated decrease in lifespan was also partially normalized by treatment with AICAR, improving lifespan from  $14.0 \pm 0.6$  days to  $20.9 \pm 0.8$  days ( $p=0.0014$ ) (Fig.6B, group 1). This effect was lost when *aak-2* was knocked out ( $p=0.6728$ ) (Fig.6B, group 2), whilst loss of the MG and ROS detoxifying enzymes *glod-4* ( $p=0.002$ ) (Fig.6B, group 3) and *sod-3* ( $p=0.0025$ ) (Fig.6B, group 4) did not affect the prolongation of lifespan by AICAR. This would suggest that indicates that AICAR acts independently from direct detoxification of ROS and dicarbonyls.

The suppression of AMPK, by RNAi, prevented the AICAR improvement in lifespan under HG conditions (Fig.6C, group 1). Similar effects were also observed in *glod-4* (Fig.6C, group 2) and *sod-3* knockouts (Fig.6C, group 3). Furthermore, a double knockout of *glod-4* and *sod-3* did not affect the lifespan prolongation by AICAR under HG conditions (Fig.6D). Similar results were also found for head motility (Fig.6E) HG decreased head motility in WT to  $0.14 \pm 0.01$  mm/s ( $p=0.0239$ ), which could be almost normalized by additional AICAR treatment to  $0.18 \pm 0.01$  mm/s ( $p=0.0398$ ), while there was no effect under S conditions ( $p=0.3364$ ) (Fig.6E, group 1). This effect of AICAR was lost when *aak-2* was knocked out ( $p=0.7611$ ) (Fig.6E, group 2), but loss of *glod-4* ( $p=0.0442$ ) (Fig.6E, group 3) and *sod-3* ( $p=0.0138$ ) (Fig.6E, group 4) did not affect the AICAR effect on head motility under HG conditions.

Neuronal damage was also not affected in a similar manner. The HG mediated increase of the neuronal damage score to  $1.29 \pm 0.12$  ( $p<0.001$ ) was normalized by additional AICAR treatment to  $0.59 \pm 0.13$  ( $p=0.0007$ ), while there was no effect under S conditions (Fig.6F, group 1). This effect was again lost when *aak-2* was down-regulated ( $p=0.0758$ ) (Fig.6F, group 2), while the loss of the MG and ROS detoxifying enzymes *glod-4* ( $p=0.0002$ ) (Fig.6F, group 3) and *sod-3* ( $p=0.0002$ ) (Fig.6F, group 4) did not affect the AICAR action of structural damages under HG. Thus, the positive effects of AICAR on head motility, neuronal damage or lifespan was affected when either *glod-4* or *sod-3* were missing.

Similar data was also obtained with respect to the accumulation of reactive metabolites. ROS

formation in WT nematodes was increased to  $205.9 \pm 8.6$  AU/pixel ( $p<0.001$ ) under HG conditions and treatment with AICAR partially normalized it to  $49.4$  AU/pixel ( $p<0.0001$ ), while there was no effect under S conditions ( $p=0.9933$ ) (Fig.6G, group 1). The effect of AICAR was lost when *aak-2* was knocked out ( $p=0.8616$ ) (Fig.6G, group 2), but loss of the MG and ROS detoxifying enzymes *glod-4* ( $p<0.0001$ ) (Fig.6G, group 3) and *sod-3* ( $p<0.0001$ ) (Fig.6G, group 4) did not affect the AICAR action of ROS formation. Similar results were also obtained for MG-derived AGEs (Fig.6H).

Treatment with AICAR not only affected *sod-3* and *glod-4* independent of the accumulation of reactive metabolites, but also the expression of *atic-1* mRNA expression (Supplementary Figure 5). This effect was more pronounced in HG than under S conditions, but was most importantly lost in the absence of *aak-2*. Furthermore, knockout of *aak-2* and *sod-3* had no effect on the formation of ds-breaks under S and HG conditions (Supplementary Figure 6), suggesting that there is no effect on purine synthesis. Thus, the effect of AICAR on all parameter studied were *aak-2* dependent. Furthermore, as the effect of AICAR treatment on all parameters studied was independent of *glod-4* and *sod-3*, mitochondrial targeting by AICAR was studied to better understand the mechanism underlying the effect of AICAR.

Effect of AICAR is independent of antioxidant defense pathways

HG mediated lifespan reduction in WT nematodes (Supplementary Figure 7A, group 1) was inhibited by AICAR, as well as rotenone. However, co-administration of AICAR plus rotenone did not affect lifespan, even under HG conditions. Thus, rotenone alone can substitute for AICAR under HG conditions. It is likely that the rotenone effect is distal from AICAR mediated AMPK activation, since in the absence of *aak-2* (Supplementary Figure 7A, group 2) the protective effect of AICAR is lost, whilst the effect of rotenone was not abrogated. Nevertheless, the effect of rotenone, as was the case with AICAR, was independent of the two major detoxifying enzymes *glod-4* (Supplementary Figure 7A, group 3) and *sod-3* (Supplementary Figure 7A, group 4). The

hypothesis that the AICAR and AMPK dependent effect on lifespan was mediated by mitochondrial ROS production (and not detoxification) was supported by the effect of the antioxidant BHA, which prolonged the lifespan of WT (Supplementary Figure 7B, group 1) and could even in the absence of *aak-2* (Supplementary Figure 7B, group 2) prolong lifespan, which was also independent of *glod-4* (Supplementary Figure 7B, group 3) and *sod-3* (Supplementary Figure 7B, group 4). The life prolonging effect of AICAR was independent of *glod-4* ( $p=0.492$ ) and *sod-3* ( $p=0.274$ ) but dependent of *aak-2* ( $p=0.040$ ) (Fig.7A). Further, the lifespan prolonging effect of rotenone was independent of *aak-2* ( $p=0.254$ ), *glod-4* ( $p=0.390$ ) and *sod-3* ( $p=0.276$ ) (Fig.7B). Further treatment of AICAR treated nematodes with rotenone had no effect on the lifespan and was independent of *aak-2* ( $p=0.276$ ), *glod-4* ( $p=0.291$ ) and *sod-3* ( $p=0.237$ ) (Fig.7C). The effect of BHA was independent of *aak-2* ( $p=0.299$ ), *glod-4* ( $p=0.118$ ) and *sod-3* ( $p=0.334$ ) (Fig.7D). The combined treatment with AICAR and BHA did not improve the lifespan further and was independent of *aak-2* ( $p=0.067$ ), *glod-4* ( $p=0.230$ ) and *sod-3* ( $p=0.174$ ) (Fig.7E). It is important to note that the effect of rotenone and BHA were exclusively present in HG treated nematodes, indicating that not basal, mitohormesis enabling ROS, but rather HG induced excessive ROS production is responsible for the HG effects observed.

## DISCUSSION

This study identified C55F2.1 as the *C. elegans* homologue for the mammalian enzyme ATIC. In contrast to mice and humans [(27);(28)], where HG is associated with increased genomic DNA damage, especially DNA double strand breaks, but also interchain crosslinks and DNA-protein crosslinks [(17)], there was no evidence of genomic DNA damage being significantly associated with the glucose effects in the model under HG conditions studied. Thus, the HG induced upregulation of *atic-1* is not needed for improving DNA repair in response to HG and a possible physiological benefit of an *atic-1* overexpression thus remains unknown. However only genomic DNA damage was studied, which in the nematode is dependent upon the RecA homologue [(29)], which does not exclude, that

mitochondrial DNA damage might play a role in HG mediated complications, too. Previous studies have shown in *C. elegans* that reactive metabolites preliminarily target mitochondrial proteins [(30);(31);(32);(33);(34)] and that mitochondrial DNA repair, involving *exo-3*, are important in the regulation response to increased production of reactive metabolites[(19)]. Future studies are needed to address the role of mitochondrial DNA damage and repair in the HG exposed nematode.

Nevertheless, inhibiting *atic-1* expression resulted under HG conditions in an unchanged development of DNA double strand breaks compared to S conditions and an increase of ds-breaks compared to ctrl. RNAi conditions. This indicates, that even in the nematode, not only the RecA homologue [(29)], but also purine synthesis is important. Under HG conditions the baseline purine synthesis is sufficient to ensure baseline DNA repair.

The findings of this study are more consistent with an important role of the ATIC-AICAR pathway in AMPK regulation of mitochondrial dysfunction, resulting in the generation of reactive metabolites and the subsequent increase in neuronal dysfunction and/or damage and reduction of lifespan. This is supported by three lines of evidence. First, the effect of *atic-1* inhibition and the effect of AICAR administration were entirely dependent on the action of *aak-2*, and independent of the classical ROS scavenging and MG detoxifying activities of *sod-3* and *glod-4*. Second, rotenone, targeting the mitochondrial complex I could normalize lifespan [(35)], independent of *aak-2*, *sod-3* and *glod-4*. Thus it could be hypothesized that AICAR/AMPK normalizes mitochondrial dysfunction in the presence of HG, since AICAR addition could not improve lifespan in the presence of rotenone. Third, the antioxidant BHA also improved the effects of HG induced events. In the presence of BHA neither AICAR, nor *aak-2*, *sod-3* or *glod-4* were required for the defense against the HG effects.

These findings would suggest that rotenone was able to reduce mitochondrial superoxide formation, thereby protecting against the effects of HG induced metabolite accumulation and neuronal damage. This is in contrast to a study in mice, which showed that mitochondrial ROS formation

inhibited AMPK and reduced STZ-diabetes induced renal damage [(9)]. A possible explanation for this difference could be the very fine homeostatic ROS response in different organisms [(11)]. While a certain dose of ROS might be protective in one model system, it might be detrimental in another [(14)]. This holds true in *C. elegans* since the protective ROS signal requires *aak-2* [(36);(37)]. A potential master regulator for this might be *daf-2*, which also regulates AMPK [(38)] and in turn, and consistent with, the concept of mitohormesis causing an adaptive, life prolonging effect involving a crosstalk with L-proline metabolism [(37)]. Future studies are required to determine the relative contribution of this crosstalk to the protective effect observed.

Such crosstalk would also affect the the complex cell-cell interactions that occur in protecting against the effects of HG. The downregulation of *atic-1* by RNAi treatment resulted in protection of head motility and structural neuronal damage, despite the fact that the RNAi treatment does not reach neuronal cells, as shown previously by others and in our model system [(39);(40)]. Thus, the non-neuronal cells affected by the RNAi could send sufficient warning signals to the neuronal cells to prepare to defend themselves against glucotoxic effects. Alternatively, HG could change the function of the non-neuronal cells, which after having acquired a dysfunctional phenotype send signals to neuronal cells, leading to their damage. Future studies would be required to distinguish between these two possibilities and determine the cell type responsible for the RNAi effect(s) which have been described.

The induction of *atic-1* by HG did not result in depletion of AICAR. The physiological capacity of *atic-1* in *C. elegans* seems to be sufficient to ensure purine synthesis and the basal concentration of AICAR was not affected by HG. In addition the physiological concentration of AICAR measured in the nematodes was at the lower detection limit and far below the AICAR concentrations needed to pharmacologically to induce AMPK activity [(41)]. Nevertheless, even though not important for the system studied here, downregulation of *atic-1* increased AICAR, consistent with a constant basal turnover of AICAR by *atic-1* and the defense against HG seen when pharmacological doses of AICAR were used. This subsequently resulted in a

reduction of ROS [(21)], MG-dependent AGEs and neuronal dysfunction. It remains unknown whether the AICAR mediated effects of *atic-1* downregulation are targeting the mitochondrial complex I alone or whether the AICAR mediated reduction of *atic-1* mRNA expression is also involved. However, it can be concluded that the major effect of the ATIC-AICAR pathway is towards the correction of mitochondrial dysfunction. Interestingly, loss of *sod-3* or *glod-4* did not impair the ATIC-AICAR effect in this setting, compatible with a model of protection against ROS and dicarbonyls not on the level of detoxification, but rather by addressing the mitochondrial dysfunction dependent generation of these metabolites.

## EXPERIMENTAL PROCEDURES

### Cloning and bacterial overexpression of *atic-1*

The ATIC homologue C55F2.1b was cloned using cDNA of wild-type *C. elegans* (RNeasy Micro Kit, Qiagen, Hilden, Germany; First Strand cDNA Synthesis Kit for RT-PCR, Roche Diagnostics, Mannheim, Germany) with primers carrying a BamHI and KpnI restriction site, respectively (forward-primer: 5'-CGA GGA TCC TGA AAT GAC CGA CGG AAA ATC AC-3'; reverse primer: 5'- AAA GGT ACC GTG TGG AAG AGA CGA AGT CCA GT-3'). The 1955 bp fragment was then ligated in frame into the vector pVH10.05 (kindly provided by H. Hutter) between the neuronal F25.B.3 promoter and the GFP-tag for a neuronal overexpression. For a ubiquitous overexpression, the ribosomal promoter Prps-5 was cloned via PstI/BamHI from the vector L4453 (kindly provided by Andrew Fire, Addgene plasmid #1655) into the plasmid pPB95.85 (Andrew Fire, Addgene plasmid #1498). In a second step, the PCR product was ligated in frame into the vector between the ribosomal promoter and the GFP-tag via BamHI/KpnI. Restriction enzymes and ligase were used following the manufactures instructions (New England Biolabs, Frankfurt, Germany). Before further using the plasmids, the sequence was proved by DNA sequencing.

### Generation of transgenic *C. elegans* by micro-injection and genomic integration

The plasmids pPB95.85+*atic-1* [Prps-5::C55F2.1b::GFP] and pVH10.05+ *atic-1* [F25.B3.3::C55F2.1b::YFP] were co-injected to the gonads of adult *pha-1* hermaphrodites together with pBX, carrying wild-type *pha-1* [(42);(43)]. 2-3  $\mu$ L were injected with a micromanipulator (LN Mini 25, Luigs und Neumann, Ratingen, Germany) in each worm (50 ng/mL *pha-1* + 50 ng/mL of the gene of interest in Tris pH 7,5) with a freshly pulled injection needle (Modell P-97, Sutter Instruments, Novata, CA, Germany) [(42);(44)]. The injected nematodes were then cultivated at 25°C to select for *pha-1* positive individuals. Two independent strains were obtained for the ubiquitous *atic-1* expression (VH2190: *pha-1*(e2123) hdEx574[Prps-5::C55F2.1b::GFP;*pha-1*(+)] and VH2191: *pha-1*(e2123) hdEx575[Prps-5::C55F2.1b::GFP;*pha-1*(+)] and two strains for a nuclear overexpression (VH2199: *pha-1*(e2123) hdEx576 [F25.B3.3::C55F2.1b::GFP;*pha-1*(+)] and VH2202: *pha-1*(e2123) hdEx577 [F25.B3.3::C55F2.1b::GFP;*pha-1*(+)]). Further experiments with extrachromosomal strains were performed at 25°C to maintain the selection pressure.

Genomic integration was achieved by UV-treatment. Freshly starved nematodes containing ideally about 50% transgenic nematodes were transferred to fresh plates and incubated at 25°C. After 1-2 days the plates were UV-exposed (UV Crosslinker FB-UVXL-1000, Fisher Scientific, 300 J/m<sup>2</sup>). After 1h rest healthy looking L4 larvae were transferred to fresh plates, each 4-5 worms per plate and starved at 15°C. To isolate the expected F2-generation for each strain 600 nematodes were isolated and cultivated at 15°C. Plates with 100% positive fluorescence were selected and the homozygous animals were outcrossed 3 times with wild-type nematodes (N2) (CGC, Minneapolis, MN, USA). VH2199 could be successfully integrated to achieve the strain VH2202: Is [F25.B3.3::C55F2.1b::GFP;*pha-1*(+)].

### *C. elegans* maintenance

Wild-type (N2 Bristol), the *sod-3* mutant strain VC433 [*sod-3*(*gk235*)X.], the AMPK k.o. mutant strain RB754 [*aak-2*(*ok524*)X], *glo-1* mutant strain

VC343 [*glod-4*(*gk189*)III.] and the pan-neuronal GFP-expressing strain NW1229 [*Prgef-1::GFP*(*evIs111*)] [(45)] were kindly provided by the *Caenorhabditis Genetics Center* (University of Minnesota, Minneapolis, MN, USA).

*C. elegans* were cultured on 60 mm NGM (nematode growth medium) plates on an OP50 lawn (*Caenorhabditis Genetics Center*, University of Minnesota, Minneapolis, MN, USA) and were transferred to FUDR-plates (300  $\mu$ g/mL 5-fluorodesoxyuridine, Sigma-Aldrich, Taufkirchen, Germany) on day 1 of adulthood for the respective experiments. The feeding method was used for the evaluation of RNAi-treatment (I/C-plates: NGM plus 1 mM isopropyl- $\beta$ -D-1-thiogalactopyranoside (IPTG) and 25  $\mu$ g/mL carbenicillin) with *Escherichia coli* HT115 expressing RNAi for *aak-2*, *atic-1*, *glod-4*, *sod-3* or control RNAi, respectively (provided by the Fire Lab *C. elegans* Vector Kit (Principal Investigator: Andrew Fire, Addgene, Cambridge, MA, USA)). The nematodes were transferred to new plates daily in the RNAi experiments.

For high glucose stimulation, the worms were treated daily with 150  $\mu$ L of a 400 mmol/L glucose solution for 5 days. One hundred fifty microliter of 400 mmol/L glucose solution achieved to a intracellular glucose concentration of 14 mmol/L in the nematode [(31)].

### Determination of lifespan

In lifespan assays the nematodes were cultivated on FUDR- or I/C-plates under standard (S) or high glucose (HG) conditions [(30)], leading to glucose concentrations of 5.5 mmol/L (99 mg/dL) and 13 mmol/L (234 mg/dL) in whole worm extracts, respectively [(31)]. Where indicated 150  $\mu$ L AICAR, BHA and rotenone were added in a concentration of 1 mM AICAR, 25  $\mu$ M BHA and 100 nM rotenone, respectively. The nematodes were regarded as dead if they did not move after repeated stimulus. Animals were excluded if they crawled away from the plate, crept into the agar or contained internally hatched larvae. Experiments were performed at least in triplicates with 60 animals each.

The lifespan experiments with the tgATIC mutant nematodes (VH2190) were performed at 15°C in

order to exclude *pha-1* dependent effects. Nematodes without fluorescence were used as controls. The experiments with the GFP-expressing strain NW1229 at 25°C to maintain the selected pressure. All other experiments were performed at 20°C.

### Quantification of gene expression

mRNA was isolated (RNeasy Micro Kit, Qiagen, Hilden, Germany) and transcribed to cDNA (First Strand cDNA Synthesis Kit for RT-PCR, Roche Diagnostics, Mannheim, Germany) followed by quantitative real-time PCR by the second derivate maximum method (Lightcycler, Roche Diagnostics, Mannheim, Germany). Primers were used as follows (Thermo Electron, Ulm, Germany): *atic-1*: 5'-GGA AGA GAC GAA GTC CAG TAT GA-3' and 5'-CAG CAA ACA GGA GTT GTF ATG AG-3', *tbg-1* (reference sequence): 5'-TGA TGA CTG TCC ACG TTG GA-3' and 5'-CGT CAT CAG CCT GGT AGA ACA-3' [(46)].

### Evaluation of neuronal damage

Structural damage was determined using a semi quantitative four-staged classification scheme in a blinded procedure [(47)]. The pan-neuronal GFP-expressing strain NW1229 [(45)] and the pan neuronal *atic-1::GFP* fusion protein overexpressing strain VH2202 were visualized by fluorescence microscopy, respectively. At least 20 nematodes were scored (score 0: healthy, no damage; score 1: minor damage; score 2: major damage; 3: extended loss of neuronal structure and dead animals, these were excluded). To assess head motility as a functional parameter, video analysis was performed at day 12 of adulthood (Moticam 1000, Beyersdörfer, Mandelbachtal, Germany). Relative head motility was calculated with a worm tracking software (WormTracker 4.0, Thomas Bornhaupt, Neustadt/ Weinstraße).

### Quantification of ROS and MG-derived AGEs

ROS were detected by oxidation of the O<sub>2</sub>-sensitive hydroethidine to ethidium [(48)]. MG-derived AGEs were detected by immunostaining with a mouse primary antibody (AGE06B, Biologo, Kronshagen, Germany) and visualised by an Alexa Fluor-labelled goat secondary antibody

### Protective Effect of AICAR under High Glucose

(Invitrogen A11002, Thermo Fisher, Rockford, IL, USA). ROS and MG-derived AGEs were quantified by confocal laser scanning microscopy [(30)] and calculated by mean pixel intensities with ImageJ software [(49)]. ROS measurement by quantification of H<sub>2</sub>O<sub>2</sub> concentration was shown to give similar results before [(48)].

### Quantification of DNA damage

DNA damage was determined by alkaline comet assay [(50)]. Nematodes were treated with HBBS-Buffer (1x Hank's balanced salt solution (Sigma-Aldrich, Darmstadt, Germany), 20nM EDTA, 10% DMSO pH8) and triturated with a glass pistil to isolate the *C. elegans* cells. The isolated cells were mixed with low melting point agarose and the mixture was loaded on an agar-coated microscope slide. The slides were immersed in ice-cold lysis solution (2.3 M NaCl, 100 mM EDTA, 10 mM Trizma base, 1% Triton X-100, 10% DMSO) at 4°C for 3 hours. The electrophoresis was performed 25 min at 24 V in electrophoresis buffer (33 mM NaOH, 200 mM EDTA). After electrophoreses, the slides were washed with neutralization buffer (0.4M Tris) and stained with DAPI (1 µg/mL). Quantification [(51); (52); (53)] was performed with a fluorescence microscope.

### Determination of AICAR levels in *C. elegans*

AICAR was determined in whole worm extracts. A pellet with approximately 800 nematodes was homogenized in M9 medium (22 mM KH<sub>2</sub>PO<sub>4</sub>, 42 mM Na<sub>2</sub>HPO<sub>4</sub>, 86 mM NaCl, pH7) by using a Bullet Blender Blue (Next Advance, Inc., Burden Lake Road, New York USA). Protein concentration was determined by using bovine serum albumin as standard. Before analysis the samples were diluted with aqua distilled to a total protein concentration of 1 mg/mL. To a 180 µL aliquot of diluted *C. elegans* were added 20 µL of 50 µM Thymin-d4 internal standard (Cambridge Isotopes, Tewksbury, MA, USA) and were filtrated with a centrifuge filter (Merck Millipore, Darmstadt, Germany) with a pore size of 0.1 µm. On a Quattro Ultima triple quadrupole mass spectrometer (Micromass, Manchester, UK) equipped with an electrospray ion source and a Micromass MassLynx data system according to Hartmann [(54)] with some modifications and the admission of AICAR, was performed the liquid

chromatography. Optimized Multiple Reaction Monitoring (MRM) experiment was performed on the most abundant ion transition ( $m/z$  259 – 127), which was identified by direct infusion of AICAR (Sigma-Aldrich, Darmstadt, Germany). Argon as collision gas, collision with an energy of 14 eV, it was operated in positive ion mode with a needle voltage of 3.15 kV. The system was equipped with a preceded C18 2.0x4 mm precolumn cartridge (Phenomenex, Aschaffenburg, Germany) and a Phenomenex Aqua C18 column (2.0x250 mm, 5  $\mu$ m particle size, Aschaffenburg, Germany). The chromatographic run was performed at 100  $\mu$ L/min with a gradient profile between 0.05 M acetic acid (pH 2.8) [eluent A] and 0.05 M acetic acid (pH 2.8) and methanol (1:1, v/v) [eluent B]. The gradient started at 100% [A], held isocratic for 2.0 min, increased to 100% [B] in 8.0 min, switch to 100% [A] in 1.5 min and re-equilibrated for 8.5 min at 100% [A]. 20 min was the overall run time and 20  $\mu$ L the injection volume. Concentrations were calculated by signal AICAR towards signal internal standard ratio and a four-point calibration curve (0 – 0.5  $\mu$ M).

#### Determination of AMPK Activity

AMPK Activity was determined in whole worm extracts by an AMPK Activity Assay (Cat# CY-1182, CycLex) [(55)]. A pellet with approximately 1000 nematodes was homogenized in lysis medium (50 mM HEPES, 50 mM KCl, 1 mM EDTA, 1mM EGTA, 5 mM  $\beta$ -glycerol phosphate, protease inhibitor cocktail (Complete, Roche), 50 mM NaF, 1 mM sodium orthovanadate, 5 mM sodium pyrophosphate and 0.2 mM PMSF) by using a Bullet Blender Blue (Next Advance, Inc., Burden Lake Road, New York USA). Protein concentration was determined by using bovine serum albumin as standard. 10 $\mu$ L Sample was mixed with 90 $\mu$ L Kinase Reaction Buffer (50  $\mu$ M ATP) and was incubated at 37°C for 45 minutes. The wells were washed five times with Wash Buffer. Pipette 100  $\mu$ L of Anti-Phospho-mouse monoclonal Antibody into the wells and incubate for 30 minutes at room temperature. Wash the wells five times, add 100 $\mu$ L Substrate Reagent and incubate for 15 minutes at room temperature. Add 100 $\mu$ L of Stop Solution to the well and measure absorbance by 450 nm.

#### Determination of AICAR formyltransferase activity

AICARFT was determined by initial appearance of tetrahydrofolate at 298 nm as described by Black [(56)] employing a thermostatic spectrometer. The cuvette contained 32.5  $\mu$ M of Tris-HCl (pH 7), 5  $\mu$ M of  $\beta$ -mercaptoethanol, 25  $\mu$ M of KCl, 0.101  $\mu$ M 10-formyl-tetrahydrofolate and enzyme, it was filled up to 0.950 mL under N<sub>2</sub> at 25°C. First the non-enzymatic rate was recorded for 10 min and was later abstracted from the initial rate obtained after added 0.05 mL of 1.01 mM AICAR. All educts was prepared from degassed H<sub>2</sub>O and were N<sub>2</sub> saturated since the blank rate was very sensitive to the amount of oxygen in the solutions. The reaction mixture for the recombinant C55F2.1 protein was mixed prior to the addition of the human AICARFT/IMPCHase enzyme and subsequently mixed again.

#### Determination of methylglyoxal production

MG concentration was measured in whole *C. elegans* lysate, as described by Töttemeyer [(57)]. The lysate was prepared by using a Bullet Blender Blue (Next Advance, Inc., Burden Lake Road, New York USA) and transferred to tubes and stored at -20°C until the assay was performed. MG was assayed colorimetrically using 2,4-dinitrophenolhydrazine (2,4-DNPH). In the assay, standard (10  $\mu$ L containing 0-10 nM of MG) and sample were added to the wells, then 70  $\mu$ L of distilled water plus 30  $\mu$ L of 0.1% 2,4-DNPH in 2 M HCl was added. After 15 min at room temperature, 140  $\mu$ L of 10% NaOH was added. After a further incubation of 10 min at room temperature the absorbance was measured at 540 nm. The recombinant ATIC protein (Abnova, Neihu District, 114 Taiwan) was mixed with 1mM dihydroxyacetone phosphate (DHAP) in 50mM Imidazole-HCl (pH7) and incubated 30 min at 30°C, to produced MG.

#### Statistical analyses

Statistical analyses were performed by Excel 2010 (Microsoft, Redmond, WA, USA) and StatView 5.0 (SAS Institute, Cary, NC, USA). The difference between two groups was analyzed by unpaired Student's t-tests and  $p < 0.05$  was considered to be significant,  $p < 0.01$  highly

significant and  $p < 0.001$  extremely high significant. Analysis of variance (ANOVA) was used for comparisons of multiple groups and Fisher's

protected least significant difference (PLSD) post hoc tests were used for additional between group comparisons.

**Acknowledgements:** We kindly thank Dr. Harald Hutter, Simon Fraser University, Department of Biological Sciences, Canada for the support and teaching us to create transgenic nematodes and the Fire Lab, Departments of Pathology and Genetics, Stanford University School of Medicine for creating the plasmids. Further, we thank Kathrin Schmidt for her excellent technical assistance.

This study was supported by the German Research Foundation (DFG), 'SFB1118, TP C06 Reactive metabolites as cause of diabetic complications' (MMe, CR, TF, SH, PPN) and 'SFB1158', TP A03 (PPN).

**Conflict of interest:** The authors declare that they have no conflicts of interest with the contents of this article.

**Author Contributions:** CR, MMe, AS performed experiments and analyzed data. CR, MMe, TF and PPN designed studies. CR, MMe, TF, JO, HH, SH and PPN wrote the manuscript and discussed. All authors reviewed the results and approved the final version of the manuscript.

## REFERENCES

1. J. M. Corton, J. G. Gillespie, S. A. Hawley, D. G. Hardie, 5-aminoimidazole-4-carboxamide ribonucleoside. A specific method for activating AMP-activated protein kinase in intact cells? *Eur. J. Biochem.* **229**, 8 (1995).
2. S. A. Hawley *et al.*, 5'-AMP activates the AMP-activated protein kinase cascade, and Ca<sup>2+</sup>/calmodulin activates the calmodulin-dependent protein kinase I cascade, via three independent mechanisms. *J Biol Chem.* **270**, 6 (1995).
3. S. P. Davies, N. R. Helps, P. T. Cohen, D. G. Hardie, 5'-AMP inhibits dephosphorylation, as well as promoting phosphorylation, of the AMP-activated protein kinase. Studies using bacterially expressed human protein phosphatase-2C alpha and native bovine protein phosphatase-2AC. *FEBS Lett.* **377**, 6 (1995).
4. M. Suter *et al.*, Dissecting the role of 5'-AMP for allosteric stimulation, activation, and deactivation of AMP-activated protein kinase. *J Biol Chem.* **281**, 10 (2006).
5. X. M. Song *et al.*, 5-Aminoimidazole-4-carboxamide ribonucleoside treatment improves glucose homeostasis in insulin-resistant diabetic (ob/ob) mice. *Diabetologia* **45**, 9 (2002).
6. R. Bergeron *et al.*, Effect of 5-aminoimidazole-4-carboxamide-1-beta-D-ribofuranoside infusion on in vivo glucose and lipid metabolism in lean and obese Zucker rats. *Diabetes* **50**, 7 (2001).
7. E. S. Buhl *et al.*, Chronic treatment with 5-aminoimidazole-4-carboxamide-1-beta-D-ribofuranoside increases insulin-stimulated glucose uptake and GLUT4 translocation in rat skeletal muscles in a fiber type-specific manner. *Diabetes* **50**, 7 (2001).
8. M. A. Iglesias *et al.*, AICAR administration causes an apparent enhancement of muscle and liver insulin action in insulin-resistant high-fat-fed rats. *DIABETES* **51**, 9 (2002).
9. L. L. Dugan *et al.*, AMPK dysregulation promotes diabetes-related reduction of superoxide and mitochondrial function. *Journal of Clinical Investigation* **132**, 12 (2013).
10. N. B. Ruderman, D. Carling, M. Prentki, J. M. Cacicedo, AMPK, insulin resistance, and the metabolic syndrome. *J Clin Invest* **123**, 9 (2013).
11. M. Ristow, K. Schmeisser, Mitohormesis: Promoting Health and Lifespan by Increased Levels of Reactive Oxygen Species (ROS). *Dose Response* **12**, 54 (2014).
12. B. Onken, M. Driscoll, Metformin induces a dietary restriction-like state and the oxidative stress response to extend *C. elegans* Healthspan via AMPK, LKB1, and SKN-1. *Plos One* **5**, 13 (2010).
13. A. Schlernitzauer *et al.*, Chicoric acid is an antioxidant molecule that stimulates AMP kinase pathway in L6 myotubes and extends lifespan in *Caenorhabditis elegans*. *PLoS One* **8**, 11 (2013).
14. M. Ristow, S. Schmeisser, Extending life span by increasing oxidative stress. *Free Radic Biol Med* **51**, 20 (2011).
15. P. T. Mungai *et al.*, Hypoxia Triggers AMPK Activation through Reactive Oxygen Species-Mediated Activation of Calcium Release-Activated Calcium Channels *Mol Cell Biol.* **31**, 15 (2011).
16. D. Kukidome *et al.*, Activation of AMP-Activated Protein Kinase Reduces Hyperglycemia-Induced Mitochondrial Reactive Oxygen Species Production and Promotes Mitochondrial Biogenesis in Human Umbilical Vein Endothelial Cells. *Diabetes* **55**, 8 (2006).
17. D. J. Xavier *et al.*, Assessment of DNA damage and mRNA/miRNA transcriptional expression profiles in hyperglycemic versus non-hyperglycemic patients with type 2 diabetes mellitus. *Mutation Research* **776**, 13 (2015).

18. J. Kasznicki, R. Krupa, J. Błasiak, J. Drzewoski, Association between polymorphisms of the DNA repair genes XRCC1 and hOGG1 and type 2 diabetes mellitus in the Polish population. *Pol Arch Med Wewn* **119**, 6 (2009).
19. A. Schlotterer *et al.*, Apurinic/aprimidinic endonuclease 1, p53, and thioredoxin are linked in control of aging in *C. elegans*. *Aging Cell* **9**, 420-432 (2010).
20. H. Vlassara, P. M.R., Diabetes and advanced glycation endproducts. *Journal of Internal Medicine* **151**, 14 (2002).
21. S. L. Habib, A. Yadav, D. Kidane, R. H. Weiss, S. Liang, Novel protective mechanism of reducing renal cell damage in diabetes: Activation AMPK by AICAR increased NRF2/OGG1 proteins and reduced oxidative DNA damage. *Cell Cycle* **15**, 11 (2016).
22. S. Bhatt *et al.*, Preserved DNA Damage Checkpoint Pathway Protects against Complications in Long-Standing Type 1 Diabetes. *Cell Metab* **22**, 32 (2015).
23. S. Tewari, J. M. Santos, R. A. Kowluru, Damaged mitochondrial DNA replication system and the development of diabetic retinopathy. *Antioxidants & Redox Signaling* **17**, 12 (2012).
24. V. Rani, G. Deep, R. K. Singh, K. Palle, U. C. Yadav, Oxidative stress and metabolic disorders: Pathogenesis and therapeutic strategies. *Life Sciences* **148**, 11 (2016).
25. J. Blasiak *et al.*, DNA damage and repair in type 2 diabetes mellitus. *Mutation Research* **554**, 8 (2004).
26. A. Sliwinska, J. Blasiak, J. Kasznicki, J. Drzewoski, In vitro effect of gliclazide on DNA damage and repair in patients with type 2 diabetes mellitus (T2DM). *Chemico-Biological Interactions* **173**, 7 (2008).
27. F. G. Ghiraldini, A. C. Crispim, M. L. Mello, Effects of hyperglycemia and aging on nuclear sirtuins and DNA damage of mouse hepatocytes. *Molecular biology of the cell* **24**, 10 (2013).
28. S. Tornovsky-Babeay *et al.*, Type 2 diabetes and congenital hyperinsulinism cause DNA double-strand breaks and p53 activity in  $\beta$  cells. *Cell Metabolism* **19**, 13 (2014).
29. N. O'Neil, A. Rose, DNA Repair. *WormBook*, ed. *The C. elegans Research Community*, 12 (2006).
30. M. Morcos *et al.*, Glyoxalase-1 prevents mitochondrial protein modification and enhances lifespan in *Caenorhabditis elegans*. *Aging Cell* **7**, 260-269 (2008).
31. A. Schlotterer *et al.*, *C. elegans* as model for the study of high glucose-mediated life span reduction. *Diabetes* **58**, 2450-2456 (2009).
32. A. Bierhaus *et al.*, Methylglyoxal modification of Nav1.8 facilitates nociceptive neuron firing and causes hyperalgesia in diabetic neuropathy. *Nature Medicine* **18**, 7 (2012).
33. T. Fleming, P. P. Nawroth, Reactive metabolites as a cause of late diabetic complications. *Biochem Soc Trans.* **42**, 3 (2014).
34. T. Brenner *et al.*, Methylglyoxal as a new biomarker in patients with septic shock: an observational clinical study. *Critical Care* **18**, 11 (2014).
35. S. Schmeisser *et al.*, Neuronal ROS signaling rather than AMPK/sirtuin-mediated energy sensing links dietary restriction to lifespan extension. *Molecular Metabolism* **2**, 11 (2013).
36. T. J. Schulz *et al.*, Glucose restriction extends *Caenorhabditis elegans* life span by inducing mitochondrial respiration and increasing oxidative stress. *Cell Metabolism* **4**, 13 (2007).
37. K. Zarse *et al.*, Impaired insulin/IGF1 signaling extends life span by promoting mitochondrial L-proline catabolism to induce a transient ROS signal. *Cell Metab.* **15**, 17 (2012).

38. R. P. Vázquez-Manrique *et al.*, AMPK activation protects from neuronal dysfunction and vulnerability across nematode, cellular and mouse models of Huntington's disease. *Human Molecular Genetic* **25**, 16 (2016).
39. M. Mendler *et al.*, Reduction in ins-7 gene expression in non-neuronal cells of high glucose exposed *Caenorhabditis elegans* protects from reactive metabolites, preserves neuronal structure and head motility, and prolongs lifespan. *Journal of diabetes and its complications* **31**, 304-310 (2017).
40. L. Timmons, D. L. Court, A. Fire, Ingestion of bacterially expressed dsRNAs can produce specific and potent genetic interference in *Caenorhabditis elegans*. *Gene* **263**, 10 (2001).
41. W. W. Winder, Can Patients with Type 2 Diabetes Be Treated with AMPK-Activators? *Diabetologia* **51**, 4 (2008).
42. C. C. Mello, J. M. Kramer, D. Stinchcomb, V. Ambros, Efficient gene transfer in *C.elegans*: extrachromosomal maintenance and integration of transforming sequences. *The EMBO journal* **10**, 3959-3970 (1991).
43. H. Schnabel, R. Schnabel, An Organ-Specific Differentiation Gene, pha-1, from *Caenorhabditis elegans*. *Science* **250**, 686-688 (1990).
44. M. Granato, H. Schnabel, R. Schnabel, pha-1, a selectable marker for gene transfer in *C. elegans*. *Nucleic acids research* **22**, 1762-1763 (1994).
45. Z. Altun-Gultekin *et al.*, A regulatory cascade of three homeobox genes, ceh-10, ttx-3 and ceh-23, controls cell fate specification of a defined interneuron class in *C. elegans*. *Development* **128**, 1951-1969 (2001).
46. B. Schumacher *et al.*, *C. elegans* ced-13 can promote apoptosis and is induced in response to DNA damage. *Cell Death Differ* **12**, 153-161 (2005).
47. M. Mendler, A. Schlotterer, M. Morcos, P. P. Nawroth, Understanding diabetic polyneuropathy and longevity: what can we learn from the nematode *Caenorhabditis elegans*? *Experimental and clinical endocrinology & diabetes : official journal, German Society of Endocrinology [and] German Diabetes Association* **120**, 182-183 (2012).
48. M. Mendler *et al.*, daf-16/FOXO and glod-4/glyoxalase-1 are required for the life-prolonging effect of human insulin under high glucose conditions in *Caenorhabditis elegans*. *Diabetologia* **58**, 393-401 (2015).
49. M. D. Abramoff, P. J. Magelhaes, S. J. Ram, Image Processing with ImageJ. *Biophotonics Int.* **11**, 36-42 (2004).
50. A. Dhawan, M. Bajpayee, K. P. A., D. Parmar, PROTOCOL FOR THE SINGLE CELL GEL ELECTROPHORESIS / COMET ASSAY FOR RAPID GENOTOXICITY ASSESSMENT. *ITRC: THE SCGE/ COMET ASSAY PROTOCOL*, 10 (2003).
51. S. Park, S. Choi, B. Ahn, DNA Strand Breaks in Mitotic Germ Cells of *Caenorhabditis elegans* Evaluated by Comet Assay. *Molecules and Cells* **39**, 6 (2016).
52. S. Imanikia *et al.*, The application of the comet assay to assess the genotoxicity of environmental pollutants in the nematode *Caenorhabditis elegans*. *Environ Toxicol Pharmacol* **45**, 5 (2016).
53. N. I. Dmitrieva, K. Cuib, D. A. Kitchaev, K. Zhaob, M. B. Burg, DNA double-strand breaks induced by high NaCl occur predominantly in gene deserts. *Proc Natl Acad Sci U S A.* **108**, 5 (2011).
54. S. Hartmann *et al.*, Comprehensive detection of disorders of purine and pyrimidine metabolism by HPLC with electrospray ionization tandem mass spectrometry. *Clinical Chemistry* **52**, 11 (2006).
55. CycLex<sup>(C)</sup>, AMPK Kinase Assay Kit. *User's Manual*.

56. S. L. Black, M. J. Black, J. H. Mangum, A rapid assay for 5-amino-4-imidazolecarboxamide ribotide transformylase. *Analytical Biochemistry* **90**, 4 (1978).
57. S. Töttemeyer, N. A. Booth, W. W. Nichols, B. Dunbar, I. R. Booth, From famine to feast: the role of methylglyoxal production in *Escherichia coli*. *Molecular Microbiology* **27**, 10 (1998).

## FOOTNOTES

The abbreviations used are: AGE, advanced glycation end-product; AICAR, 5-Aminoimidazole-4-carboxamide ribonucleotide; AICARFT, 5-Aminoimidazole-4-carboxamide ribonucleotide formyltransferase; AMP, adenosine monophosphate; AMPK, adenosine monophosphate-kinase; ATIC, AICAR-transformylase/IMP cyclohydrolase; ATP, adenosine triphosphate; AU, arbitrary units; BHA, butylhydroxyanisole; *C. elegans*, *Caenorhabditis elegans*; Ctrl., Control; DNA, deoxyribonucleic acid; GFP, green fluorescent protein; GLO, Glyoxalase; GLOD, glyoxalase domain containing; HG, high glucose; k.o., knockout; MG, methylglyoxal; NGM, nematode growth medium; RNAi, RNA interference; ROS, reactive oxygen species; S, standard; SOD, superoxide dismutase; tg, transgenic; WT, wild-type.

**FIGURE LEGENDS**

**FIGURE 1:** Effect of HG on the *C. elegans* homologue C55F2.1b (A) Effect of C55F2.1b overexpression on AICARFT activity. AICARFT activity was detected by formation of 10-formyl-tetrahydrofolate in *C. elegans* lysates of WT and transgenic C55F2.1b nematodes as described in Methods. Human recombinant protein catalyzed this reaction. Data represents mean  $\pm$  SD of 4 independent experiments, each with 30 nematodes per group are shown. (B) Effect of C55F2.1b overexpression on MG production. *C. elegans* were cultivated under S conditions. MG production was detected by spectroscopy in lysates of WT, transgenic C55F2.1b nematodes and recombinant human protein incubated with 2,4-dinitrophenolhydrazine, as described in Methods. Data represents mean  $\pm$  SD of 2 experiments, each with 30 nematodes per group. (C) HG induced C55F2.1b mRNA expression. *C. elegans* were cultured under standard (S) and high glucose (HG) conditions, mRNA expression was quantified by RT-PCR and normalized to *tbp-1* and S as described in Methods. Data represents mean  $\pm$  SD of 3 independent experiments, each performed in triplicates. (D) Effect of HG stimulation on ATIC activity in WT and transgenic C55F2.1b nematodes as described in Methods. Data represent mean  $\pm$  SD of 1 experiment with 1000 nematodes per group. \* $p < 0.05$ , \*\* $p < 0.01$  and \*\*\* $p < 0.001$  calculated using the unpaired Student's t-test.

**FIGURE 2:** Effect of *atic-1* overexpression on lifespan and neuronal damage (A) Lifespan of tgATIC (VH2190, dashed line) and control (solid line) nematodes under S conditions. Shown is 1 representative of 3 independent experiments, each with 60 nematodes per group. (B) Head mobility was determined as described in Methods. WT and tgATIC (VH2193) *C. elegans* were kept under S and HG conditions as indicated. Data represents mean  $\pm$  SD of 3 independent experiments, each with 15 nematodes per group. Head motility under S conditions is defined as 0. (C) Neuronal structure was visualized by a pan-neuronal-specific GFP reporter and was scored in a blinded procedure as described in Methods. Data represents mean  $\pm$  SD of 4 independent experiments, each with 12 nematodes per group. \* $p < 0.05$  and \*\* $p < 0.01$  calculated using the unpaired Student's t-test. (D) Neuronal structure was identified by a pan-neuronal-specific GFP reporter. Shown are representative pictures of a single nematodes

**FIGURE 3:** Effect of *atic-1* downregulation on lifespan, neuronal damage and reactive metabolites accumulation in *C. elegans* (A) Effect of *atic-1* downregulation on lifespan of control (ctrl., solid line) and *atic-1* RNAi (dashed line) feeding plates under HG conditions. 1 representative experiment out of 3 independent experiments is shown, each with 60 nematodes per group. (B) Head motility was determined by video analysis as described in Methods under control RNAi, or *atic-1* RNAi, each under S and HG conditions. Data represents mean  $\pm$  SD of 3 independent experiments, each with 15 nematodes per group. (C) Neuronal structure was visualized by a pan-neuronal-specific GFP reporter and was scored in a blinded procedure as described in Methods, under S or HG conditions, with control or *atic-1* RNAi. Data represents mean  $\pm$  SD of 3 independent experiments, each with 12 nematodes per group. (D) ROS formation was detected by confocal laser scanning microscopy of ethidium-labeled *C. elegans*, as described in Methods, under S and HG conditions. Data represents mean  $\pm$  SD of 3 independent experiments, each with 20 nematodes per group. (E) MG-derived AGEs accumulation was detected by immunostaining and quantified as described in Methods. Data represents mean  $\pm$  SD of 3 independent experiments, each with 20 nematodes per group. \* $p < 0.05$ , \*\* $p < 0.01$  and \*\*\* $p < 0.001$  calculated using the unpaired Student's t-test.

**FIGURE 4:** Effect of *atic-1* regulation on AICAR levels determined in a whole body extract and on DNA damage (A) AICAR concentration in whole *C. elegans* extracts was determined as described in Method. WT *C. elegans* were grown on ctrl. or *atic-1* RNAi feeding plates, tgATIC nematodes were grown on control plates. Data represents mean  $\pm$  SD of 3 independent experiments. Comet assay from WT *C. elegans* treated with bleomycine (positive control) (B), cultivated under S (C) and HG (D) condition. (E) WT and tgATIC mutant *C. elegans* were cultivated under S and HG conditions. WT *C. elegans* were cultivated on ctrl. or *atic-1* RNAi feeding plates, respectively. Data represents mean

$\pm$  SD of 6 independent experiments, each with 70 nematodes per group. \* $p < 0.05$ , \*\* $p < 0.01$  and \*\*\* $p < 0.001$  calculated using the unpaired Student's t-test.

**FIGURE 5:** Effect of *atic-1* downregulation on lifespan, neuronal damage and reactive metabolites in *C. elegans* in an AMPK dependent manner (A) Effect of *atic-1* downregulation on lifespan of control (ctrl., solid line) or *atic-1* RNAi (dashed line) feeding plates under HG conditions. 1 representative experiment of 3 independent experiments is shown, each with 60 nematodes per group. (B) Head motility was determined by video analysis as described in Methods under control, or *atic-1* RNAi, each under S and HG conditions. Data represents mean  $\pm$  SD of 3 independent experiments, each with 15 nematodes per group. (C) ROS formation was detected by confocal laser scanning microscopy of ethidium-labeled *C. elegans*, as described in Methods, under S and HG conditions. Data represents mean  $\pm$  SD of 3 independent experiments, each with 20 nematodes per group. (D) MG-derived AGE accumulation was detected by immunostaining and the mean pixel was quantified, as described in Methods. Data represents mean  $\pm$  SD of 3 independent experiments, each with 20 nematodes per group. \*\* $p < 0.01$  and \*\*\* $p < 0.001$  calculated using the unpaired Student's t-test.

**FIGURE 6:** Effect of AICAR under HG conditions is dependent on AMPK and independent of glyoxalase-1 and superoxide dismutase-3 *C. elegans* were cultivated under S and HG conditions and treated with 1 mM AICAR, respectively. (A) Effect of HG and AICAR on AMPK activity over time. Effect of HG and AICAR (1 mM) treatment on AMPK activity under S and HG conditions in WT nematodes after 5 day treatment. Data represents mean  $\pm$  SD, each with 1000 nematodes per group. (B) Effect of AICAR on the lifespan of different mutant nematodes as indicated in the Figure. Data represents mean  $\pm$  SD of 3 independent experiments, each with 60 nematodes per group. (C) Lifespan of *C. elegans* grown on ctrl. RNAi and *aak-2* RNAi feeding plates respectively under HG conditions. Data represents mean  $\pm$  SD of 3 independent experiments, each with 60 nematodes per group. (D) Lifespan of *glod-4 C. elegans* grown on ctrl. and *sod-3* RNAi feeding plates, respectively under S and HG conditions. Shown are means and standard errors of 3 independent experiments, each with 60 nematodes per group. (E) Head mobility was determined by video analysis as described in Methods under S and HG conditions. Data represents mean  $\pm$  SD of 3 independent experiments, each with 20 nematodes per group. (F) Neuronal structure was visualized by a pan-neuronal-specific GFP reporter and neuronal damage was scored in a blinded procedure as described in Methods under S or HG conditions (NW1229: GFP express WT nematode). Data represents mean  $\pm$  SD of 3 independent experiments, each with 20 nematodes per group. (G) ROS formation were detected by confocal laser scanning microscopy of ethidium-labeled *C. elegans*, as described in Methods cultivated under S and HG conditions. Data represents mean  $\pm$  SD of 3 independent experiments, each with 20 nematodes per group. (H) MG-derived AGEs accumulation was detected by immunostaining and the mean pixel intensity was quantified as described in Methods. Data represents mean  $\pm$  SD of 3 independent experiments, each with 20 nematodes per group. \* $p < 0.05$ , \*\* $p < 0.01$  and \*\*\* $p < 0.001$  calculated using the unpaired Student's t-test.

**FIGURE 7:** Effect of AICAR, BHA and rotenone under HG conditions were dependent on AMPK and independent of glyoxalase-1 and superoxide dismutase-3. (A-C) Effect of treatment with 100 nM of the complex-1 inhibitor rotenone on lifespan of AICAR treated nematodes under HG conditions in WT, *aak-2*, *glod-4* and *sod-3* deficient nematodes. (D-E) Effect of treatment with 25  $\mu$ M of the antioxidant BHA on lifespan of AICAR treated nematodes under HG conditions. Data represents mean  $\pm$  SD of 3 independent experiments, each with 60 nematodes per group. \* $p < 0.05$ , \*\* $p < 0.01$  and \*\*\* $p < 0.001$  calculated using the unpaired Student's t-test.

Figure 1

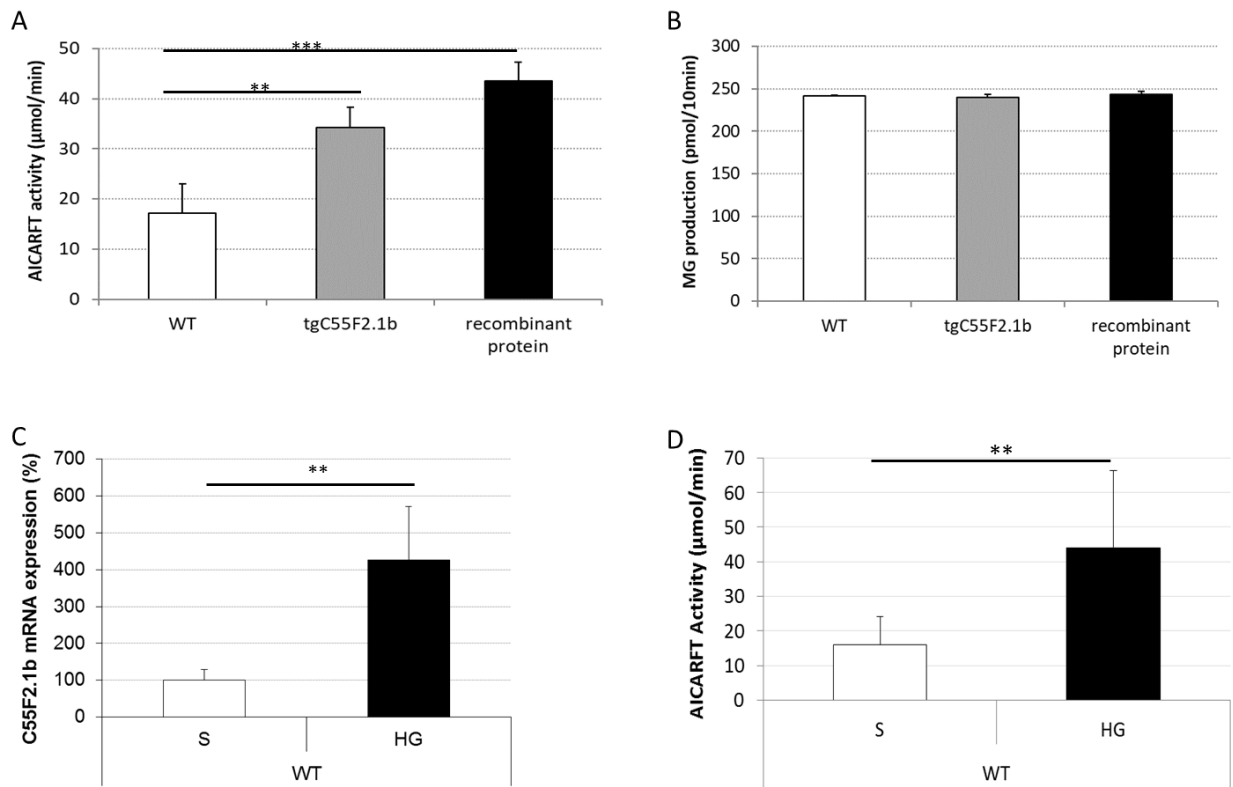


Figure 2

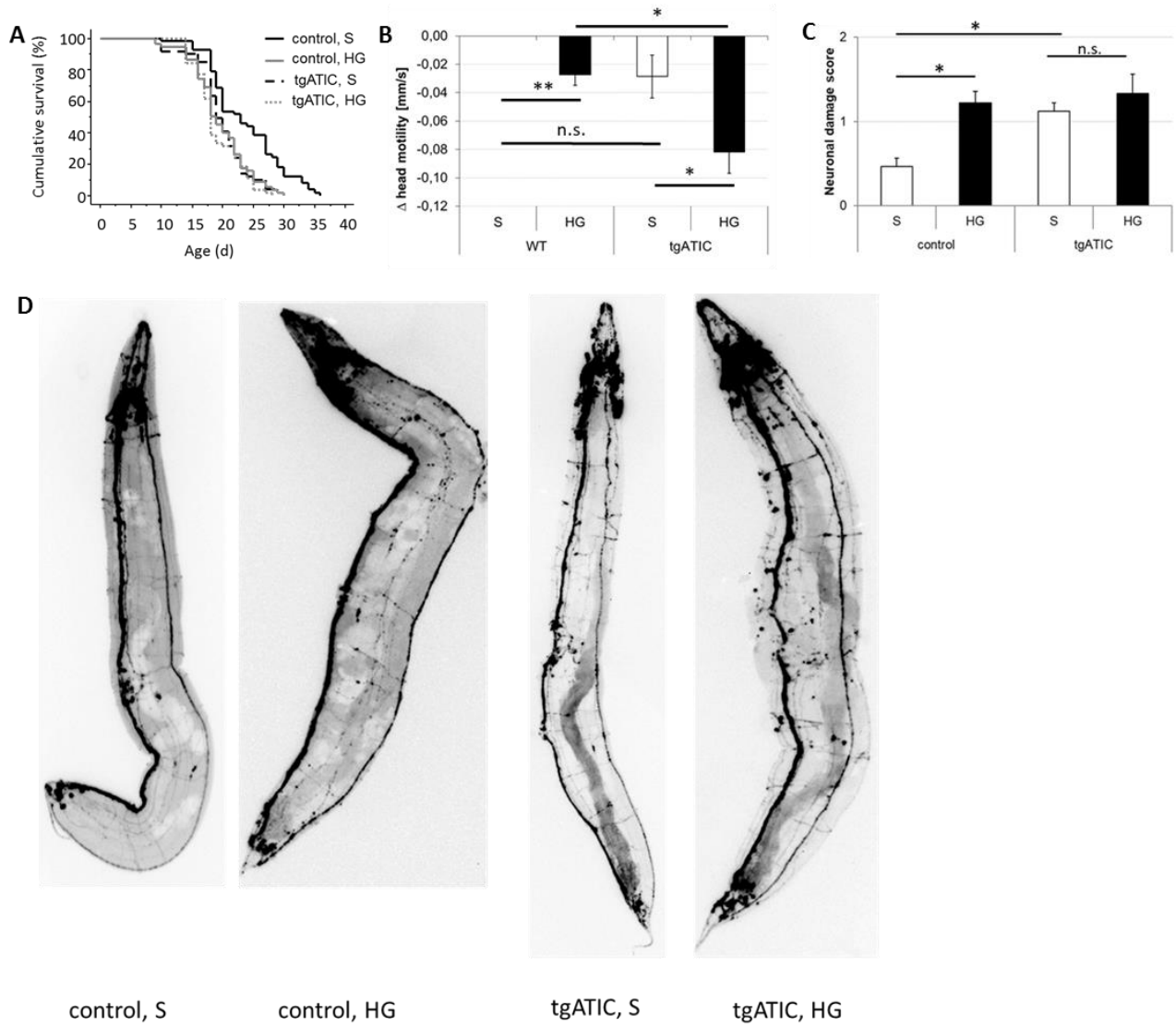


Figure 3

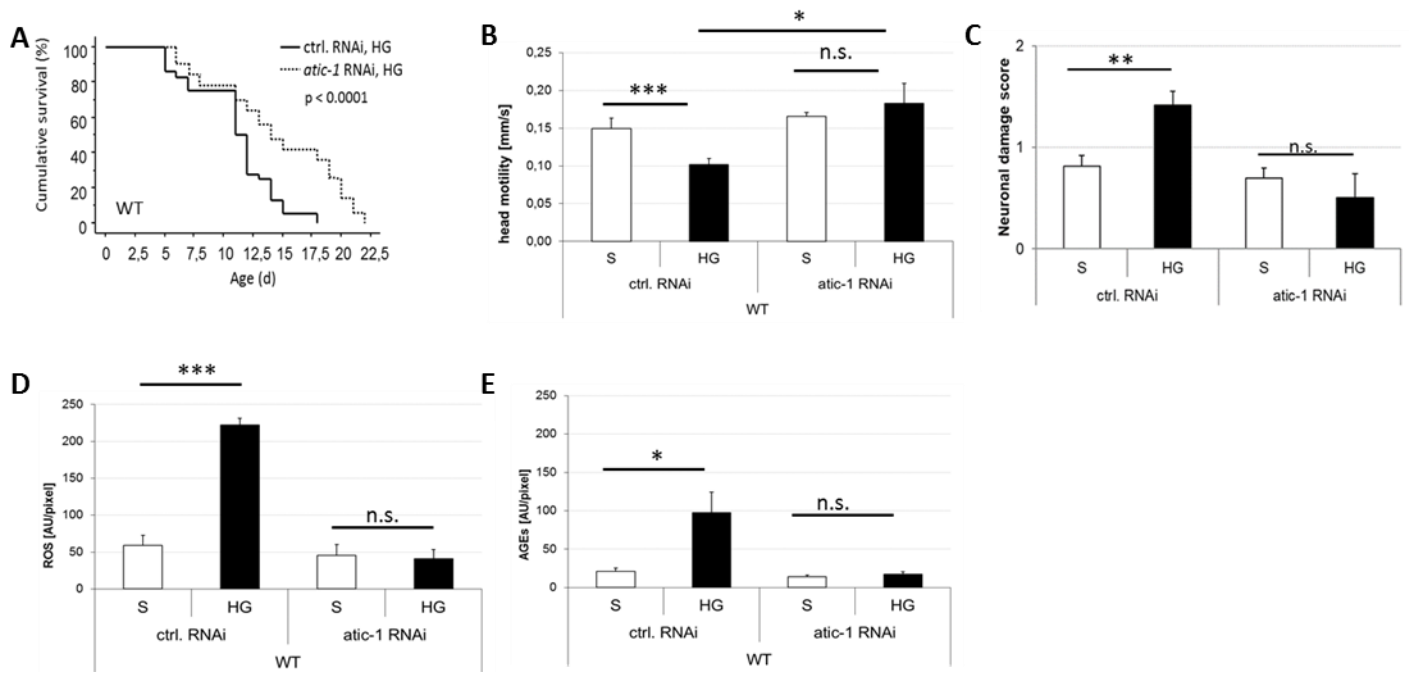


Figure 4

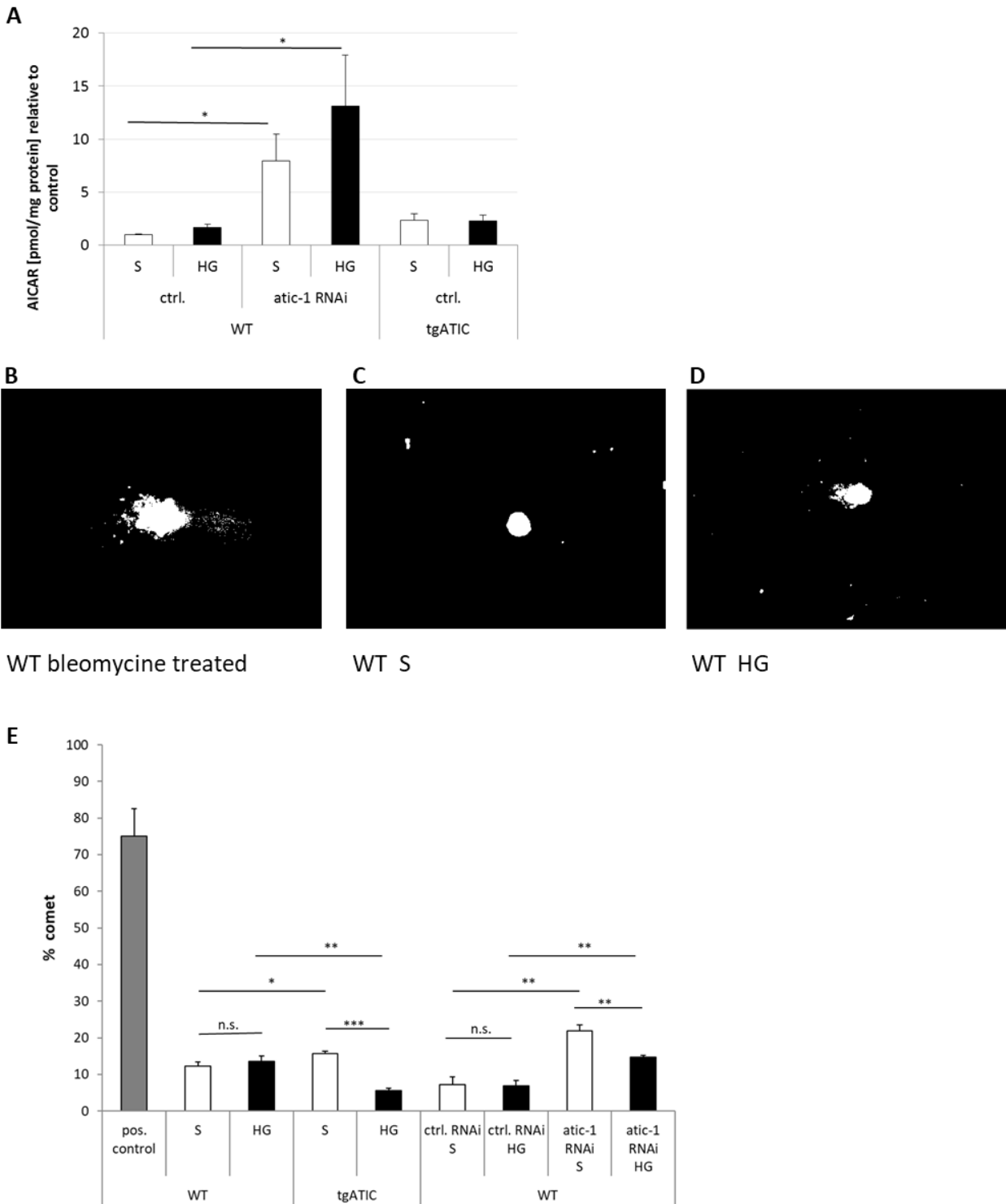


Figure 5

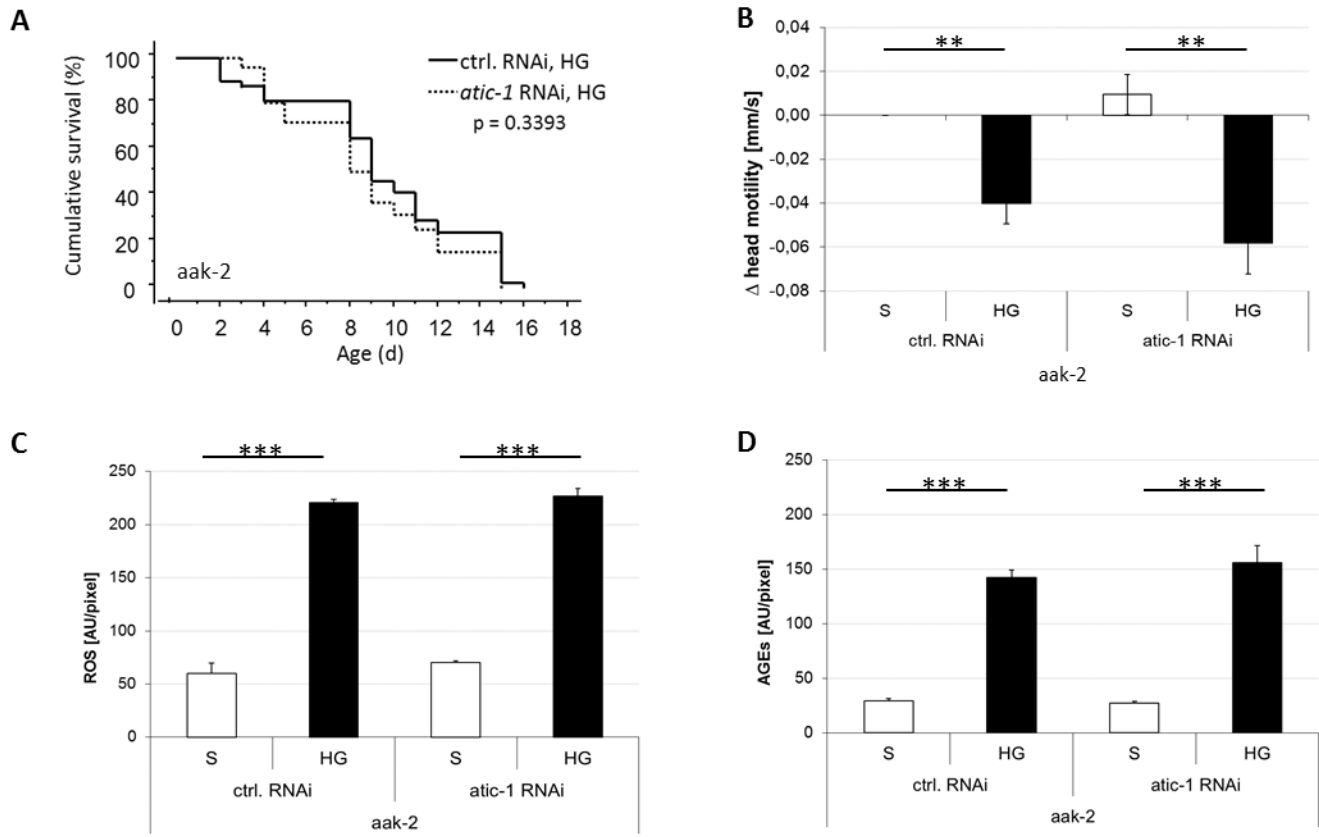


Figure 6

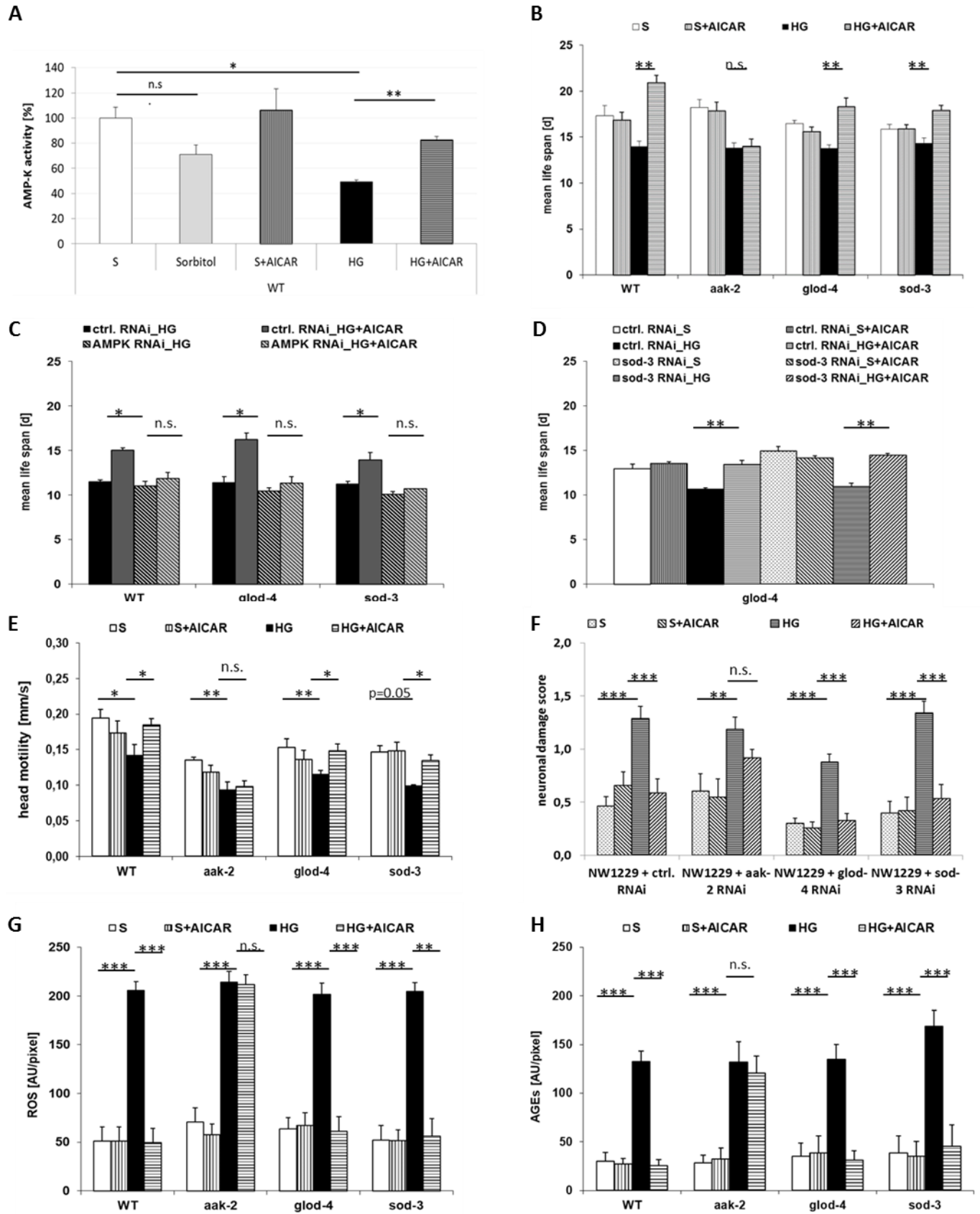
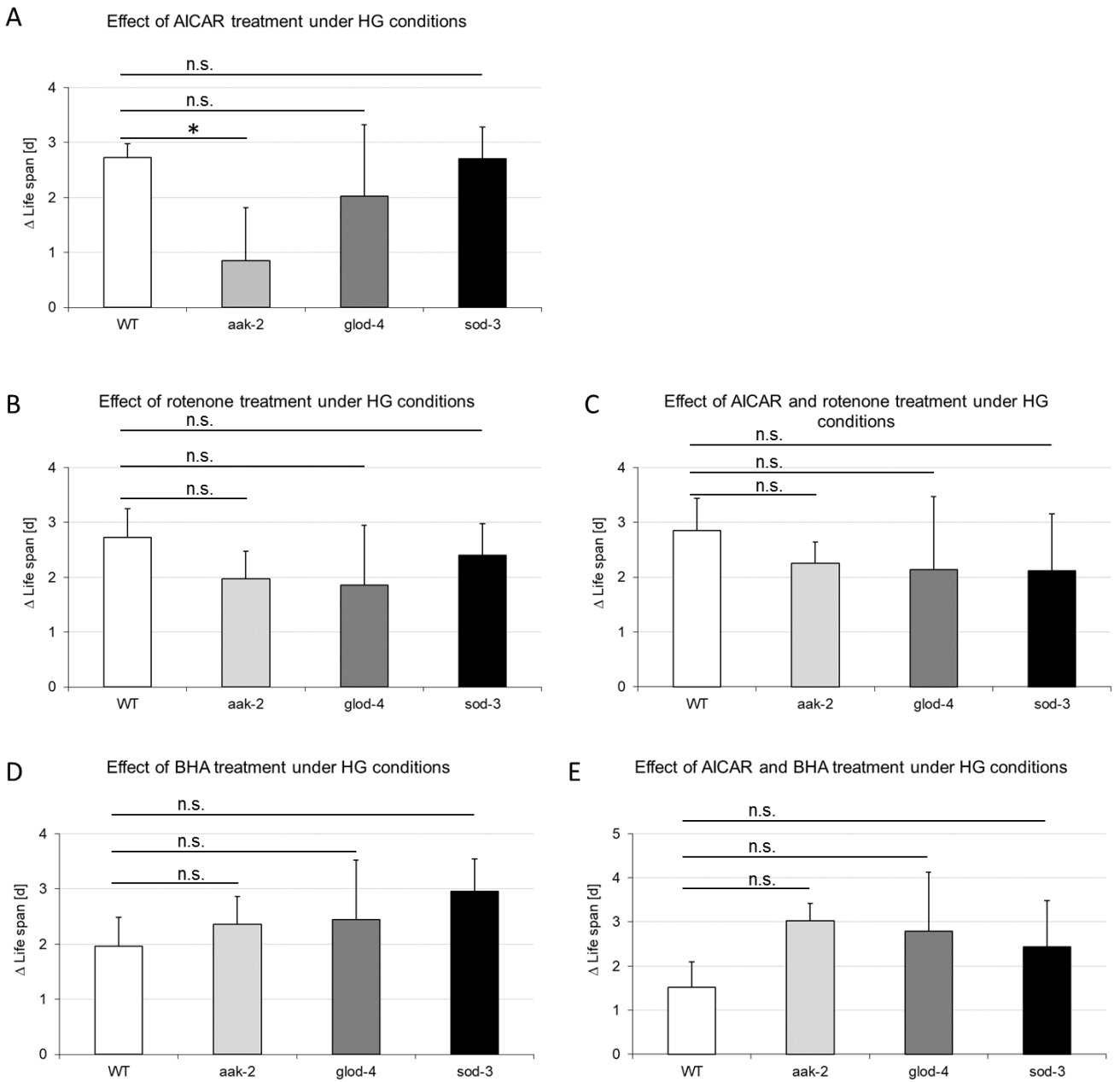


Figure 7



**High-glucose toxicity is mediated by AICAR-transformylase/IMP cyclohydrolase and mitigated by AMP-activated protein kinase in *Caenorhabditis elegans***

Christin Riedinger, Michael Mendler, Andrea Schlotterer, Thomas Fleming, Jürgen Okun, Hans-Peter Hammes, Stephan Herzig and Peter P. Nawroth

*J. Biol. Chem.* published online February 2, 2018

---

Access the most updated version of this article at doi: [10.1074/jbc.M117.805879](https://doi.org/10.1074/jbc.M117.805879)

Alerts:

- [When this article is cited](#)
- [When a correction for this article is posted](#)

[Click here](#) to choose from all of JBC's e-mail alerts